

Negatively Charged Muonium and Related Centers in Solids

Takashi U. Ito^{1*}, Wataru Higemoto^{1,2}, and Koichiro Shimomura³

¹Advanced Science Research Center, Japan Atomic Energy Agency, Tokai, Ibaraki 319-1195, Japan

²Department of Physics, Tokyo Institute of Technology, Meguro, Tokyo 152-8551, Japan

³Institute of Materials Structure Science, High Energy Accelerator Research Organization (KEK), Tsukuba, Ibaraki 305-0801, Japan

Muonium (Mu) centers formed upon implantation of μ^+ in a solid have long been investigated as an experimentally accessible model of isolated hydrogen impurities. Recent discoveries of hydridic centers formed at oxygen vacancies have stimulated a renewed interest in H^- and corresponding Mu^- centers in oxides. However, the two diamagnetic centers, Mu^+ and Mu^- , are difficult to separate spectroscopically. In this review article, we summarize established and developing methodologies for identifying Mu^- centers in solids, and review recent Mu studies on said centers supposedly formed in mayenite, oxygen-deficient $SrTiO_{3-x}$, and $BaTiO_{3-x}H_x$ oxyhydride.

1. Introduction

Hydrogen is a ubiquitous impurity in most semiconductors and insulators, which can unintentionally enter crystalline lattices during crystal growth as well as subsequent processing. The incorporated hydrogen often has a significant impact on structural and electrical properties of these materials in spite of low hydrogen solubilities.¹⁾ It is beneficial to application of Si, where hydrogen passivates dangling bonds of undercoordinated Si at vacancies, impurities, surfaces, and interfaces. Meanwhile, hydrogen can also passivate deliberate dopants by forming H-dopant complexes. It has also been recognized that hydrogen isolated from other defects has an electrical activity, involving all allowed charge states: H^+ , H^0 , and H^- . The isolated hydrogen often shows amphoteric behavior, acting as both deep donor and acceptor in accordance with the Fermi level position in the band gap.²⁾ It can also behave as shallow donor, which has been observed in several oxides, such as ZnO,³⁾ or as shallow acceptor. Because of these complex electrical activities, a detailed understanding of hydrogen and related defects is vital for application of host materials. However, it is very difficult to experimentally characterize hydrogen in such trace quantities, particularly isolated hydrogen.

Muonium (Mu) centers formed upon implantation of μ^+ in a solid have long been used as an experimentally accessible model of hydrogen.¹⁾ Indeed, the electronic states of H and Mu centers are nearly identical, as can be seen when comparing atomic $Mu^0 (= \mu^+e^-)$ and H^0 in a vacuum: they have almost the same reduced mass. Microscopic insight into Mu centers can be obtained using the muon spin rotation, relaxation, and resonance (μ^+ SR) spectroscopy, which is analogous to the 1H nuclear magnetic resonance (NMR) spectroscopy. Technical details of the μ^+ SR method have been previously outlined in existing literature, such as Ref. [4]. Since

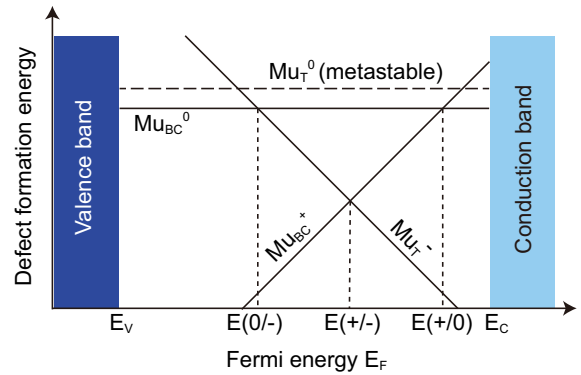


Fig. 1. (Color online) Defect-formation energy diagram for interstitial Mu in GaAs.

only a small number of muons stay in a sample at a time, the μ^+ SR method can provide information on isolated Mu centers. In principle, the electronic structures of Mu centers can be investigated more precisely than those of corresponding H centers by measuring hyperfine frequencies or chemical shifts because the gyromagnetic ratio for μ^+ is roughly three times larger than that for 1H . It should be also emphasized that the Mu centers observed may not be in global equilibrium⁵⁾ because the formation of Mu centers and the observation of their states are completed in a relatively short time scale, which is comparable to the muon lifetime $\sim 2.2 \mu s$. Therefore, the μ^+ SR spectroscopy is potentially useful for investigating excited hydrogen configurations in heavily hydrogenated compounds as well, where Mu species are expected to behave as metastable excess hydrogen and interact with preexisting hydrogen in the host lattice.⁶⁾

Historically, the Mu approach has played an important role in microscopically establishing the amphoteric behavior of isolated interstitial hydrogen in many semiconductors, such

*ito.takashi15@jaea.go.jp

as Si and GaAs. Figure 1 shows the Mu defect-formation energy diagram for GaAs obtained from comparisons with a theoretical model of H²⁾ and the experimental results for Mu.⁵⁾ This indicates that the interstitial Mu counteracts prevailing conductivity as a donor Mu⁺ or an acceptor Mu⁻. In addition, the dominant equilibrium charge state changes from positive to negative at the charge-transition level $E(+/-)$ as a function of the Fermi energy E_F . According to Van de Walle and Neugebauer, $E(+/-)$ for H should be universally pinned at a specific energy below the vacuum level.²⁾ This was experimentally confirmed by Lichti *et al.* for Mu analogs in Si, Ge, GaAs, GaP, ZnSe, and 6H-SiC.⁵⁾ The defect-formation energy diagram also suggests that the dominant equilibrium charge state is always Mu⁺ (Mu⁻) when $E(+/-)$ is in the conduction (valence) band. Indeed, such shallow donor (acceptor) behavior has been theoretically predicted for interstitial H in some oxides, nitrides, and sulfides,⁷⁻¹²⁾ as well as indirectly confirmed by observing shallow donor (acceptor) Mu states.¹³⁻²¹⁾

Recent discoveries of hydridic centers formed at oxygen vacancies (V_O) have stimulated a renewed interest in H⁻ and corresponding Mu⁻ centers in oxides. Theoretically, the most stable form of hydrogen trapped at V_O is H⁻, where doubly charged V_O^{2+} changes into singly charged H_O^+ .^{10,11,22,23)} This indicates that the substitutional H⁻ serves as a single donor in sharp contrast to the acceptor behavior of the interstitial H⁻. A large amount of O²⁻ in the host lattice can be replaced with H⁻ due to its structural stability (up to ~40% in SmFeAsO_{1-x}H_x²⁴⁾ and ~20% in BaTiO_{3-x}H_x²⁵⁾). The substitutional H⁻ is becoming more and more important as an electron dopant in oxides²⁴⁾ and a novel charge carrier for solid-state ionic conductors.²⁵⁾ However, microscopic insight into substitutional H⁻ and related defect complexes is currently limited.

The μ^+ SR spectroscopy is potentially useful for the study of Mu⁻ analog in oxides, where attention should be focused on distinguishing between Mu⁻ and Mu⁺. Generally, it is difficult to separate these diamagnetic Mu species spectroscopically because they have quasi-identical responses to the applied magnetic field B . In this review article, we summarize new and existing methodologies for identifying Mu⁻ centers. In addition, we review the recent μ^+ SR studies on said centers supposedly formed in mayenite, oxygen-deficient SrTiO_{3-x}, and BaTiO_{3-x}H_x oxyhydride upon implantation of μ^+ . Finally, we provide concluding remarks on the future prospects of Mu⁻ studies.

2. Methodologies for Identifying Mu⁻ and Related Centers

2.1 Local Structures

Computational studies on H impurities in semiconductors have revealed that correlations exist between their crystallographic sites and favorable charge states (Fig. 2).²⁶⁾ However, it is difficult to identify the structures of H-related defects due to their random distribution as well as low concentrations. Therefore, the information on the structures of Mu centers obtained from μ^+ SR spectroscopy is vital with respect

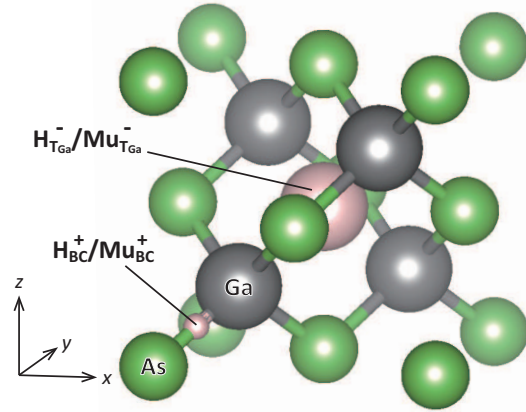


Fig. 2. (Color online) Correlations between the sites and favorable charge states of diamagnetic H/Mu centers in GaAs.²⁶⁾ The structure was drawn using VESTA.³²⁾

to identifying Mu/H charge states. The structures of paramagnetic Mu⁰ centers can be easily estimated from hyperfine anisotropies.^{27,28)} This is also the case for shallow and polaronic Mu centers, where a Mu⁺ or Mu⁻ core weakly binds an unpaired electron or hole.^{13-21,29)} Contrastingly, diamagnetic Mu[±] centers are much more difficult to characterize because they do not have unpaired electrons, and, accordingly, they lack hyperfine interactions. In such cases, magnetic-dipolar and electric-quadrupolar interactions between a muon and surrounding nuclei can be used to identify the structures of diamagnetic Mu centers. These interactions can be efficiently studied using the muon level-crossing resonance (μ LCR) technique,¹⁾ as demonstrated in heavily doped GaAs.^{30,31)}

Two paramagnetic and two diamagnetic Mu centers are primarily observed in GaAs.¹⁾ In heavily doped samples, only the diamagnetic Mu centers are detectable. Theoretical studies on H impurities²⁶⁾ suggest that they should be assigned to Mu⁻ at the tetrahedral site surrounded by Ga atoms (T_{Ga}) or Mu⁺ near the bond-center (BC) position (Fig. 2). The Mu_T⁻ and Mu_{BC}⁺ centers are theoretically stable in n -type and p -type carrier-rich environments, respectively.

Chow *et al.* investigated the diamagnetic Mu center formed in n -type GaAs (Si concentrations between 2.5×10^{18} and 5×10^{18} cm⁻³) using μ LCR and conventional transverse-field (TF) μ^+ SR techniques to establish the Mu_T⁻ state from a structural point of view.³⁰⁾ Herein, the time-integrated muon spin polarization \bar{P} was obtained in the longitudinal field (LF) configuration⁴⁾ as a function of B . The spin Hamiltonian relevant to this experiment comprises the Zeeman interactions for the muon and surrounding nuclei, the magnetic-dipolar interactions between the muon and the nuclei, and the electric-quadrupolar interactions for the nuclei that have an electric field gradient (EFG) primarily caused by the diamagnetic Mu. Resonant cross relaxation between the muon and the nuclei, observed as dips in $\bar{P}(B)$, occurs when the muon Zeeman splitting matches the separation of the combined quadrupo-

lar and Zeeman energy levels for the nuclei. The resonance position depends on the electric quadrupolar parameter Q_i for the on-resonance nucleus i and the angle θ_i between \mathbf{B} and the muon-nucleus axis. For a given Q_i and θ_i , the intensity of the resonance line is a function of the muon-nuclear dipolar coupling D_i , which is dependent on the muon-nucleus distance r_i . Chow *et al.* observed a couple of doublets in the \bar{P} spectrum under $\mathbf{B} \parallel \langle 001 \rangle$, which were assigned to the two spin-3/2 isotopes of ^{69}Ga and ^{71}Ga . Another resonance was identified at the low-field end of the spectrum, assigned to ^{75}As with spin 3/2. The small number of lines and the structure of the Ga doublets indicate that the principal axis of the EFG tensor, or the muon-Ga axis, is parallel to $\langle 111 \rangle$ at $\theta_{\text{Ga}} \sim 54.7^\circ$, which is compatible with the BC, T_{Ga} , and AB_{Ga} (antibonding to a Ga atom) sites. The r_i parameter was estimated as $r_{\text{Ga}} = 2.199(7) \text{ \AA}$ and $r_{\text{As}} = 2.72(5) \text{ \AA}$ from a combined analysis of the μLCR spectrum and the $\text{TF-}\mu^+\text{SR}$ Gaussian width as functions of \mathbf{B} . The results are consistent with the Mu^- center at the T_{Ga} site, the r_{Ga} of which is roughly 10% shorter than expected for an undistorted GaAs lattice.

The μLCR technique cannot be applied to systems that do not contain nuclei with a finite nuclear quadrupolar moment. Even in such cases, the local structures of diamagnetic Mu centers are occasionally determined via the magnetic-dipolar interactions between a muon and the surrounding nuclei. Characteristic oscillating features appear in zero field (ZF) $\mu^+\text{SR}$ spectra when the muon is dipole coupled to a small number of nuclei, thus creating an entangled a-few spin system.^{33–38} Such a state often forms in materials containing fluorine^{33–35} or hydrogen^{36–38} with relatively strong electronegativity, which causes muons to preferentially localize in their vicinity. In addition, the ^{19}F and ^1H nuclei with spin 1/2 have relatively large dipolar moments. Here we consider an entangled spin system consisting of a muon and a spin-1/2 nucleus. The powder-averaged muon spin relaxation function for the two-spin state (hereafter, referred to as 2S) in ZF can be expressed as

$$G_{2S}(t) = \frac{1}{6} + \frac{1}{6} \cos(2\pi f_d t) + \frac{1}{3} \cos(\pi f_d t) + \frac{1}{3} \cos(3\pi f_d t), \quad (1)$$

$$f_d = \frac{\mu_0 \hbar \gamma_\mu \gamma_I}{8\pi^2 d^3}, \quad (2)$$

where d is the distance between μ^+ and the spin-1/2 nucleus and γ_μ and γ_I are the gyromagnetic ratios for μ^+ ($\gamma_\mu/2\pi = 135.53 \text{ MHz/T}$) and the nucleus ($\gamma_I/2\pi = 42.58 \text{ MHz/T}$ for ^1H or 40.08 MHz/T for ^{19}F), respectively (Fig. 3).^{34,39} The muon-nucleus distance, d , obtained by fitting eq. (1) is useful with respect to estimating the local structure of a diamagnetic Mu center. This method was applied to identify an $\text{H}^- \text{-Mu}^-$ complex supposedly formed in the $\text{BaTiO}_{3-x}\text{H}_x$ oxyhydride upon implantation of μ^+ by Ito *et al.*,⁶ as reviewed in Section 3.3.

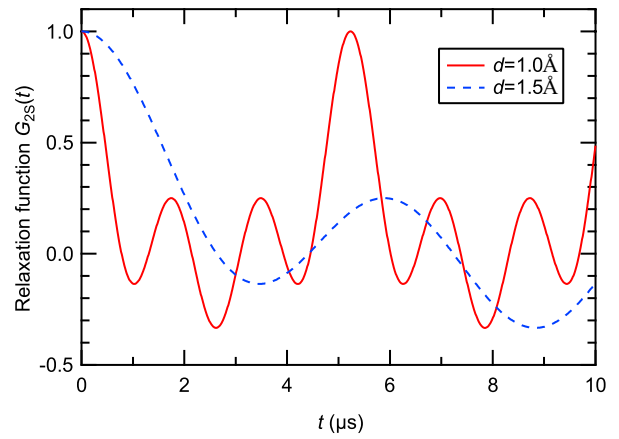


Fig. 3. (Color online) ZF muon spin relaxation function $G_{2S}(t)$ for the 2S state with $\gamma_I/2\pi = 42.58 \text{ MHz/T}$ (muon- ^1H complex). The solid and dashed curves correspond to the configurations with $d = 1.0 \text{ \AA}$ and 1.5 \AA , respectively.

2.2 Thermal Properties

As the temperature increases, the Mu site changes and/or charge-state transitions are thermally activated. Characteristic energies relevant to these processes are obtained from the temperature dependences of diamagnetic and paramagnetic Mu amplitudes and muon spin relaxation rates.¹⁾ The Mu species involved can be identified by mapping these energies to theoretically allowed transitions. The H/Mu defect-formation energy diagram, such as Fig. 1, obtained from first-principles calculations provides potential candidates for the transitions that are linked to Mu sites and charge states. In low-carrier systems, final Mu states can be different from promptly formed Mu states, which may be reached via a delayed process with a time constant comparable to the muon lifetime $\sim 2.2 \mu\text{s}$. The radio frequency (RF) $\mu^+\text{SR}$ technique is suitable for investigating such final states, as demonstrated in the studies of Mu centers in Si, Ge, and GaAs.^{5,40–43}

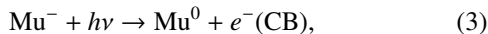
Longitudinal T_1 relaxation is often linked to cyclic charge-state transitions between Mu^0 and Mu^- or Mu^+ in thermal equilibrium. Chow *et al.* established that the Mu defect in heavily doped n -type GaAs:Si serves as a deep recombination center via the observation of a $\text{Mu}_T^{-/0}$ charge cycle.⁴⁴ The longitudinal relaxation rate $1/T_1$ associated with the $\text{Mu}_T^{-/0}$ dynamics is expressed as a function of λ_{-0} , λ_{0-} , A_μ , and B , where λ_{-0} and λ_{0-} are the rates of conversion for $\text{Mu}_T^{-} \rightarrow \text{Mu}_T^0$ and $\text{Mu}_T^0 \rightarrow \text{Mu}_T^{-}$, respectively, and A_μ is the hyperfine coupling constant for Mu_T^0 . The λ_{-0} (hole capture rate) exhibits Arrhenius-like behavior with an activation energy of $1.66(7) \text{ eV}$. This value is approximal to that of the band gap in GaAs, suggesting that a band-gap excitation governs this process. Contrastingly, the λ_{0-} (electron capture rate) is independent of temperature and much larger than the λ_{-0} . This is expected since the electron-carrier concentration is nearly temperature-independent in heavily doped n -type GaAs.

The T_1 relaxation can also occur when a $\text{Mu}^{+/0}$ charge cy-

cle is activated. The values and behavior of charge-transition rates associated with this process in intrinsic Si are considerably different from those of λ_{-0} and λ_{0-} in heavily doped n -type GaAs.⁴⁵⁾ This suggests that the charge state of diamagnetic Mu species involved in a Mu-charge cycle can be distinguished by carefully investigating the charge-transition rates.

2.3 Photo-Detachment of the Second Electron from Mu^-

The optical excitation of electrons trapped at point defects to the conduction band (CB) is a useful method of investigating the corresponding defect levels formed in the band gap. Such a technique, combined with μ^+ SR, is also helpful with respect to distinguishing between Mu^- and Mu^+ in semiconductors. The photoexcitation of the second electron from Mu^- to the CB causes a paramagnetic Mu^0 center, which can be described as



where $h\nu$ denotes a photon with energy corresponding to the optical excitation of the second electron to the CB minimum. The photogenerated Mu^0 center is detectable using conventional μ^+ SR techniques due to the strong hyperfine interactions.

Shimomura *et al.* conducted optical μ^+ SR experiments to identify the Mu_T^- acceptor in n -type GaAs using a high-power pulse laser.^{46,47)} The experiments were performed at the port 2 of the RIKEN-RAL muon facility, UK, using a broadband OPO laser system pumped by a 355-nm beam from a Nd:YAG laser. The laser system was operated in pulse mode at a 25-Hz repetition rate and synchronized to the arrival of muon pulses to a single-crystalline GaAs wafer doped with $3 \times 10^{16} \text{ cm}^{-3}$ Si. The decrease in μ^+ SR asymmetry associated with the $\text{Mu}_T^- \rightarrow \text{Mu}_T^0$ conversion was recorded as a function of photon energy, which was scanned from 0.8 to 1.5 eV. Shimomura *et al.* found a broad feature centered at around 1 eV after normalizing the asymmetry decrease by laser power. This is consistent with the results obtained from the temperature dependence of RF- μ^+ SR amplitude assigned for the $\text{Mu}_T^- \rightarrow \text{Mu}_T^0 + e^-(\text{CB})$ excitation.⁴³⁾ Moreover, a sharp feature was identified at around 1.5 eV, which was attributed to the spin or charge scattering between Mu_T^- and photoexcited electrons. Subsequent experiments using circularly polarized laser light revealed that this effect depends on the polarization direction of conduction electrons with respect to the muon polarization direction; however, the exact mechanism is yet to be clarified.^{48,49)}

2.4 Chemical Shifts

Recent systematic ^1H -NMR studies in Ca and Sr-mayenites (C12A7 and S12A7) have revealed that ^1H chemical shifts are useful with respect to distinguishing nominally H^+ and H^- species.⁵⁰⁾ Mayenites comprise a class of cage-structured compounds that contain “extraframework” anions in their cages, such as O^{2-} , OH^- , H^- , and e^- .⁵¹⁾ Hayashi *et al.* prepared mayenite samples incorporating OH^- or H^- extraframe-

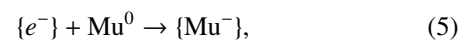
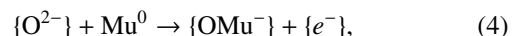
work anions with concentrations approximal to theoretical maxima and measured the isotropic chemical shifts δ_{iso} for said H species using the magic-angle-spinning technique. They obtained a δ_{iso} of +5.1 ppm (+6.1 ppm) for H^- and -0.8 ppm (-1.3 ppm) for OH^- (formally H^+) in C12A7 (S12A7) with respect to the tetramethylsilane (TMS) reference. Surprisingly, the observed values of δ_{iso} for H^- are larger than those for H^+ , falling within the typical range for the H^+ state from +20 to 0 ppm.⁵²⁾ This result suggests that the electron density around the ^1H nuclei, which is associated with the chemical-shielding effect, is larger for H^+ than H^- species in mayenites. First-principles calculations using the periodic and embedded cluster approaches successfully reproduced such electronic states as well as the $\delta_{iso}(\text{H}^-) > \delta_{iso}(\text{H}^+)$ relation. The experimental and theoretical results for δ_{iso} s are consistent with each other within 1 ppm, demonstrating that the combined approach based on ^1H chemical shift measurements and first-principles calculations is useful with respect to identifying the charge state of H species. Systematic surveying of the relation between the ^1H chemical shift and the local structure around H species has also been conducted for many oxides, ionic hydrides, and mixed-anion hydrides. The research suggests that the distance between the H species and the coordinating atoms strongly affects the chemical shift and that δ_{iso} for both H^+ and H^- is distributed in a similar range. This indicates that the H^\pm species can be separated by carefully analyzing the chemical shift; however, it does not serve as an *easy* fingerprint of the nominal charge states.

The chemical shift approach has also been applied to identify Mu^\pm species supposedly formed in C12A7: O^{2-} and C12A7: e^- upon implantation of μ^+ by Hiraishi *et al.*,⁵³⁾ as reviewed in Section 3.1.

3. Recent Mu^- Studies in Oxides

3.1 Chemical Shifts of Diamagnetic Mu Centers in Mayenite [53]

The extraframework H species in C12A7 mayenite have attracted much attention in association with persistent photoconductivity in C12A7: H^{-54}) and highly efficient ammonia synthesis using Ru-loaded C12A7: e^- .^{55,56)} Hiraishi *et al.* adopted the μ^+ SR technique to investigate the electronic structure and chemical activity of these centers using Mu analogs.⁵³⁾ Here, we focus on their attempts to distinguish extraframework OMu^- (formally Mu^+) and Mu^- species by measuring the Mu chemical shift K_μ according to the methodology outlined in Section 2.4. These species are supposedly formed in C12A7: O^{2-} and C12A7: e^- , respectively, via



where $\{X\}$ indicates an extraframework anion X in a cage.

Mu chemical shift measurements were conducted on single-crystalline samples of C12A7: O^{2-} (pristine insulator) and C12A7: e^- (electride, $n \sim 10^{21} \text{ cm}^{-3}$) in the high-TF configuration⁴⁾ at TRIUMF, Canada, using a spin-polarized sur-

face muon beam. A TF of 6 T was applied along the muon incident axis, which was nominally perpendicular to the (001) plane. For both samples, the value of K_μ was mostly independent of temperature below 300 K. The temperature-averaged K_μ was +0.3(4) ppm for C12A7:O²⁻ and +6.6(4) ppm for C12A7:e⁻ using CaCO₃ as a zero-shift reference. These results are consistent with corresponding ¹H chemical shifts, specifically $\delta_{iso} = -0.8$ ppm for C12A7:OH⁻ and $\delta_{iso} = +5.1$ ppm for C12A7:H⁻, using TMS as a reference.⁵⁰⁾ On the basis of this similarity, Hiraishi *et al.* assigned the chemical state of diamagnetic muons in the C12A7:O²⁻ and C12A7:e⁻ samples to {OMu⁻} and {Mu⁻}, respectively. However, there seems to be some ambiguity associated with the difference in the gyromagnetic ratios for μ^+ and ¹H ($\gamma_\mu/\gamma_H \sim 3.2$). Indeed, the value of K_μ for {Mu⁻} in C12A7:e⁻ is considerably smaller than expected from the ¹H chemical shift for C12A7:H⁻ ($5.1 \times 3.2 = 16$ ppm). This discrepancy was tentatively attributed to the metallic environment of Mu⁻ in the C12A7:e⁻ sample ($n \sim 10^{21}$ cm⁻³).⁵³⁾

3.2 Possible Charge-State Dynamics of Mu in Oxygen-Deficient SrTiO_{3-x} [57]

Oxygen vacancies can act as electron donors in SrTiO₃, causing a wide range of interesting phenomena, such as superconductivity⁵⁹⁾ and ferromagnetism.⁶⁰⁾ The oxygen-deficient SrTiO_{3-x} can be obtained by annealing the parent band insulator in highly reducing atmospheres. Hydrogen is often used as a reducing agent in this process. Systematic annealing studies have revealed that such a treatment does not only remove oxygen to obtain metallic SrTiO_{3-x}, but that it can also create other types of defects involving hydrogen.⁶¹⁾ The most common H-related defect in perovskite oxides is an interstitial H⁺ bound to an O²⁻ in the host lattice, which serves as a shallow donor in SrTiO₃.⁶²⁾ This behavior has also been confirmed from Mu viewpoints.^{29,63)} Contrastingly, subsequent hydrogen annealing of the metallic SrTiO_{3-x} causes a decrease in conductivity.⁶¹⁾ This contradictory behavior against the interstitial H⁺ implies that the site and charge state of hydrogen introduced by the subsequent annealing is considerably different from those of the interstitial H⁺. First-principles studies suggest that the most stable form of hydrogen in SrTiO_{3-x} is H⁻ located at the anion site, where doubly charged V_O²⁺ changes into singly charged H_O⁺.¹¹⁾

Motivated by these theoretical predictions, Shimomura *et al.* conducted μ^+ SR experiments in oxygen-deficient SrTiO_{3-x} at the D1 area of J-PARC MUSE, Japan, with the expectation that implanted muons are preferentially trapped in V_O where they form a substitutional Mu⁻ center.⁵⁷⁾ The SrTiO_{3-x} sample was prepared by reducing single-crystalline wafers of SrTiO₃ with the (110) surface according to the procedure outlined in Ref. [61]. The μ^+ SR measurements were performed using a double-pulsed surface muon beam and the DΩ1 spectrometer (maximum asymmetry ~ 0.20) in the LF geometry⁴⁾ under a weak TF of 2 mT applied perpendicular to the [110] direction.

μ^+ SR asymmetry spectra were fitted to a function com-

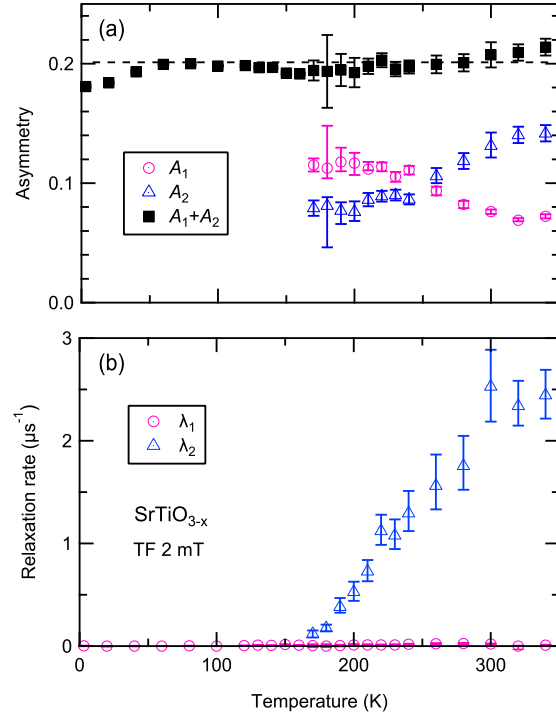


Fig. 4. (Color online) Temperature dependences of (a) the partial asymmetries A_1 and A_2 and (b) the exponential relaxation rates λ_1 and λ_2 in SrTiO_{3-x}. These values were updated from those in Ref. [57] by taking account of double-pulse correction⁵⁸⁾ in a series of fits. The dashed line indicates the maximum asymmetry for the DΩ1 μ^+ SR spectrometer.

posed of two exponentially-damped cosines with a shared diamagnetic frequency. Following [57], the fits were refined by taking into account double-pulse correction.⁵⁸⁾ Figure 4 shows the partial asymmetries A_1 and A_2 and the exponential relaxation rates λ_1 and λ_2 for the two (fast and slow) components as functions of temperature. The A_2 for the fast component was set to zero for fits below 160 K. We can find a decrease in the total diamagnetic asymmetry, $A_1 + A_2$, below ~ 50 K from the maximum value of ~ 0.20 . Similar behavior was also observed in nominally undoped SrTiO₃, where muons should stay at interstitial sites, and the asymmetry drop was attributed to the formation of shallow hydrogen-like Mu⁶³⁾ or Mu⁺-bound small polaron.²⁹⁾ This similarity implies that an interstitial Mu⁺ state is partially involved in the observed diamagnetic signal. However, the diamagnetic amplitude below 50 K is significantly larger than that in undoped SrTiO₃. Shimomura *et al.* ascribed the increased diamagnetic fraction in oxygen-deficient SrTiO_{3-x} to the hydridic Mu⁻ center formed in V_O.

The λ_2 for the fast component markedly increases with increasing temperature above 160 K. Shimomura *et al.* tentatively attributed this anomalous behavior to the activation of cyclic Mu^{-/0} charge-state transitions on the basis of similarity with the temperature dependence of $1/T_1$ in *n*-type GaAs⁴⁴⁾

(see Section 2.2). However, there seem to be some difficulties in this interpretation. In particular, the $\text{Mu}^{-/0}$ charge cycle model for n -type materials assumes that the Mu^- defect creates a deep level in the band gap and serves as a recombination center.⁴⁴⁾ However, according to computational studies, the defect level for the substitutional H^- falls in the valence band.¹¹⁾ Moreover, a characteristic energy of ~ 0.1 eV estimated from the increase in $\lambda_2(T)$ is much smaller than the band-gap energy of 3.2 eV. Accordingly, a different model may be necessary to explain the unusual exponential relaxation possibly associated with Mu-state dynamics in SrTiO_{3-x} .

3.3 Metastable Hydride-Related Center in $\text{BaTiO}_{3-x}\text{H}_x$ [6]

Oxyhydrides of perovskite titanates $\text{ATiO}_{3-x}\text{H}_x$ ($A = \text{Ba}$, Sr , and Ca) comprise a new class of hydrogen ion conductors, which can be obtained from ATiO_3 parent insulators by CaH_2 reduction.^{25,64,65)} Conventional diffraction techniques can be applied to identify the H site in $\text{ATiO}_{3-x}\text{H}_x$ since a large amount of H up to $x \sim 0.6$ can be incorporated. A combined analysis of x-ray and neutron diffraction data revealed that O^{2-} ions in the perovskite lattice are randomly substituted by H^- ions without creating any detectable amount of V_O . The substitutional H^- in $\text{ATiO}_{3-x}\text{H}_x$ is in sharp contrast with the interstitial protonic hydrogen (formally H^+) bound to an O^{2-} ion, which is a common impurity often found in ATiO_3 . Macroscopic gas analysis revealed that the hydrogen in the solid phase is mobile and exchangeable in hydrogen gas environments above $\sim 400^\circ\text{C}$. Moreover, the reduction treatment changes the parent band insulators into paramagnetic metals. These transport characteristics suggest that $\text{ATiO}_{3-x}\text{H}_x$ compounds are suitable for application in mixed electron/hydrogen ion conductors and hydrogen membranes.

Several theoretical models have been proposed regarding the stability of H species in $\text{ATiO}_{3-x}\text{H}_x$ and their kinetics.^{10,11,22,23)} These studies commonly conclude that the substitutional H^- configuration is most stable in n -type carrier-rich environments. With respect to the dynamical aspect of H in the solid phase, two types of scenarios have been proposed. One is based on the concept of correlated migration of H^- , O^{2-} , and V_O in the network of the anion site [type-I H migration, Fig. 5(a)].^{22,25,66)} The other model [type-II H migration, Fig. 5(b)] involves two metastable H configurations: the interstitial H^+ bound to O^{2-} , and two H atoms trapped at the same anion site in place of O^{2-} . The former can support rapid proton diffusion via the Grotthuss mechanism,²³⁾ and the latter can act as a hydrogen exchange center, which is expected to temporarily form due to the interaction between a substitutional H^- and an incoming interstitial H^+ . Two charge configurations, hydridic $2\text{H}^{-11)}$ and molecular H_2 ,²³⁾ have been proposed for this center.

The $\mu^+\text{SR}$ technique is useful for creating and investigating experimentally accessible models of such metastable H-related centers. This is based on the fact that the as-implanted mixture of Mu states is far from equilibrium, often involving metastable excited states.⁵⁾ Ito *et al.* conducted $\mu^+\text{SR}$ inves-

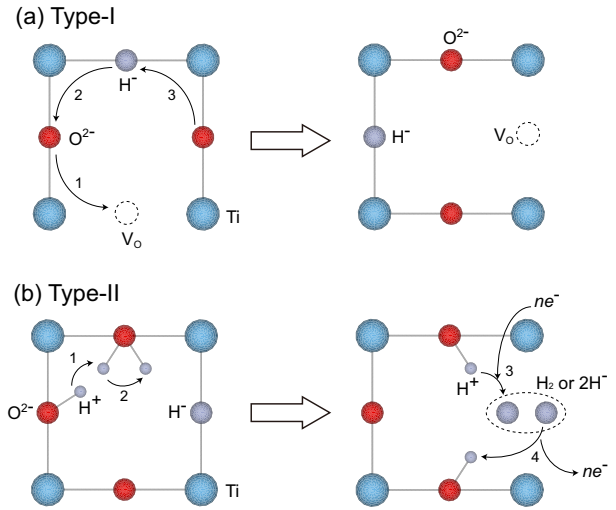


Fig. 5. (Color online) (a) Type-I and (b) type-II H migration models for $\text{ATiO}_{3-x}\text{H}_x$. The structure was drawn using VESTA.³²⁾

tigations of prototypical $\text{BaTiO}_{3-x}\text{H}_x$ to obtain microscopic insight into the metastable H configurations associated with type-II H migration using Mu as a pseudoisotope of H.⁶⁾ The $\mu^+\text{SR}$ measurements of powder samples of $\text{BaTiO}_{3-x}\text{H}_x$ ($x = 0.1, 0.2, 0.3$ and 0.5) were carried out in the D1 area of J-PARC MUSE, Japan, and in the port 2 of RIKEN-RAL, U.K., using a spin-polarized surface muon beam. Muons implanted in the samples lose their kinetic energy via electromagnetic interactions with host atoms and are then trapped in local potential minima (not necessarily in the global minimum). In $\text{BaTiO}_{3-x}\text{H}_x$, implanted muons are expected to serve as incoming excess hydrogen, creating Mu analogs of the metastable configurations involved in the type-II H migration model together with H^- in the host lattice. Information on their charge states was obtained via the local structure approach outlined in Section 2.1.

Figure 6(a) shows the time evolution of muon spin polarization $P(t)$ at 15 K in ZF for the $x = 0.3$ and 0.5 samples. The $P(t)$ curves have a damped cosine-like feature superposed on a Gaussian relaxation curve. The oscillating feature is a signature of the formation of the entangled 2S state composed of diamagnetic Mu and H. The Gaussian relaxation part is usually ascribed to muons that interact with a large number of surrounding nuclei without creating such a special magnetic coupling.⁶⁷⁾ Therefore, the two components were tentatively assigned to the metastable configurations involved in the type-II model: the 2S component for a Mu analog of the hydrogen exchange center [Fig. 6(e)] and the Gaussian component for the interstitial Mu^+ [Fig. 6(f)].

Accordingly, the ZF spectra at 15 K were fitted to the following function,

$$P(t) = p_{2S} e^{-\lambda t} G_{2S}(t; f_d) + (1 - p_{2S}) e^{-\Delta^2 t^2}, \quad (6)$$

where λ , p_{2S} , and $G_{2S}(t; f_d)$ denote the relaxation rate, the fraction, and the ZF relaxation function in eq. (1) for the

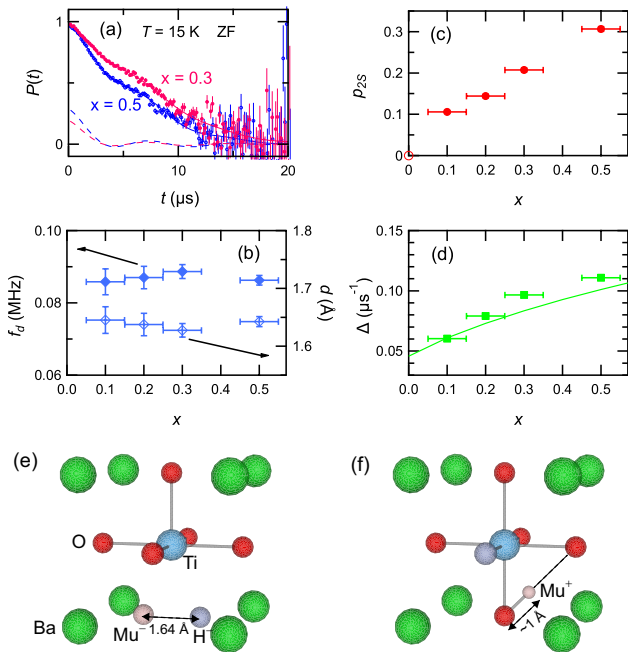


Fig. 6. (Color online) (a) ZF- μ^+ SR spectra of $\text{BaTiO}_{3-x}\text{H}_x$ ($x = 0.3$ and 0.5) at 15 K. The solid curves represent the best fits to eq. (6). The dashed curves show partial contribution from the 2S component. (b), (c), and (d): x dependences of f_d and d , p_{2S} , and Δ at 15 K in ZF. (e) and (f): the most probable atomic configurations associated with the 2S and Gaussian components. In the structure model (f) assigned to the Gaussian component, O^{2-} ions at the third nearest neighbor and further anion sites are randomly replaced by H^- with a probability of $x/3$. The structure was drawn using VESTA.³²⁾ Reproduced with some modifications from Ref. [6] ©American Physical Society.

2S state, respectively. The distance d between a muon and a nearby H can be obtained from f_d through eq. (2). d is independent of x [Fig. 6(b)], which is expected since the Mu-H structure should be robust against changes in x . The average value of $d = 1.64(1) \text{ \AA}$ is consistent with the theoretical H^- - H^- distances of 1.64 and 1.67 \AA for symmetric and asymmetric 2H^- centers in SrTiO_{3-x} ;¹¹⁾ however, this does not match $d = 0.74 \text{ \AA}$ for a molecular MuH configuration. On the basis of these results, Ito *et al.* assigned the 2S component to a hydridic (Mu^- , H^-) complex formed at V_O . Meanwhile, the x dependence of the Gaussian relaxation rate Δ associated with the interstitial Mu^+ configuration can be reproduced by calculating the rms width of the nuclear dipolar field at the interstitial Mu^+ site, as shown in Fig. 6(d) with a solid curve.

The temperature dependence of Δ for the $x = 0.5$ sample reveals that interstitial Mu^+ diffusion (activation energy $\sim 0.1 \text{ eV}$) and subsequent trapping in an unknown deep potential well occur above 100 K within the μ^+ SR time window. This re-trapping process may function as a rate-limiting step of macroscopic H transport in the $\text{BaTiO}_{3-x}\text{H}_x$ lattice. It is not taken into account in the type-II H migration model.

4. Future Prospects

The identification of Mu^- and related defects in solids remains a challenge due to the fact that an *easy* method of

separating Mu^- from Mu^+ is yet to be established. A lot of beam time is still required to scan the vast parameter space of temperature, field, and carrier concentration to accumulate indirect evidence of Mu charge states and secure overall consistency with theoretical predictions. Pulsed muon beams are beneficial for these experiments due to the capability of the high-count-rate measurements. The major drawback of the pulsed μ^+ SR method (i.e., relatively low time resolution) can be mostly overcome by using the RF resonance technique. The RF technique is also indispensable with respect to the sensitivity to the Mu final state formed via a delayed process.^{5, 40–43)} Unfortunately, the RF- μ^+ SR method has only occasionally been used for materials research, even though the majority of muon facilities support it. Obviously, further improvements of RF instruments (and their user interfaces) are vital for future Mu^- studies.

The Mu chemical shift approach reviewed in Section 2.4 and Section 3.1 is undoubtedly promising for separating Mu^- from Mu^+ ; however, it also seems to require further improvements. This approach is based on comparisons with computational and/or experimental ^1H chemical shifts. Unfortunately, the use of the different standard samples (TMS for $^1\text{H-NMR}$ ⁵⁰⁾ and CaCO_3 for μ^+ SR⁵³⁾) may have resulted in some ambiguity in said comparison. These materials were employed to set a chemical shift of zero. It should be noted that the zero shift does not necessarily mean a null chemical-shielding effect on the ^1H nuclei or muons. First-principles calculations revealed that the absolute screening constant for protons in TMS is about 30 ppm.⁶⁸⁾ This relatively high shielding results in the majority of ^1H resonances occurring downfield within 20 ppm of TMS.⁵²⁾ Meanwhile, little is known about the chemical-shielding effect on the diamagnetic Mu species in CaCO_3 . The relation between the TMS and CaCO_3 references must be clarified for establishing the Mu chemical shift strategy with respect to separating diamagnetic Mu species. The absolute screening constant for the diamagnetic Mu species in CaCO_3 may be determined with high precision by using the apparatus for the MuSEUM (Muonium Spectroscopy Experiment Using Microwave) project at J-PARC.⁶⁹⁾

Acknowledgment

Discussions and correspondence are gratefully acknowledged with K. Nishiyama, K. Fukutani, Y. Iwazaki, S. Tsuneyuki, R. Kadono, and N. Nishida.

- 1) S. F. J. Cox: Rep. Prog. Phys. **72** (2009) 116501.
- 2) C. G. Van de Walle and J. Neugebauer: Nature **423** (2003) 626.
- 3) D. M. Hofmann, A. Hofstaetter, F. Leiter, H. Zhou, F. Henecker, B. K. Meyer, S. B. Orlinskii, J. Schmidt, and P. G. Baranov: Phys. Rev. Lett. **88** (2002) 045504.
- 4) A. Yaouanc and P. Dalmas de Réotier: *Muon Spin Rotation, Relaxation, and Resonance: Applications to Condensed Matter* (Oxford University Press, 2010) 1st ed.
- 5) R. L. Lichti, K. H. Chow, and S. F. J. Cox: Phys. Rev. Lett. **101** (2008) 136403.

- 6) T. U. Ito, A. Koda, K. Shimomura, W. Higemoto, T. Matsuzaki, Y. Kobayashi, and H. Kageyama: *Phys. Rev. B* **95** (2017) 020301(R).
- 7) C. G. Van de Walle: *Phys. Rev. Lett.* **85** (2000) 1012.
- 8) S. Limpijumngong and C. Van de Walle: *Physica Status Solidi (b)* **228** (2001) 303.
- 9) C. Kılıç and A. Zunger: *Appl. Phys. Lett.* **81** (2002) 73.
- 10) Y. Iwazaki, T. Suzuki, and S. Tsuneyuki: *J. Appl. Phys.* **108** (2010) 083705.
- 11) Y. Iwazaki, Y. Gohda, and S. Tsuneyuki: *APL Mater.* **2** (2014) 012103.
- 12) J. B. Varley and V. Lordi: *Appl. Phys. Lett.* **103** (2013) 102103.
- 13) J. M. Gil, H. V. Alberto, R. C. Vilão, J. Piroto Duarte, P. J. Mendes, L. P. Ferreira, N. Ayres de Campos, A. Weidinger, J. Krauser, C. Niedermayer, and S. F. J. Cox: *Phys. Rev. Lett.* **83** (1999) 5294.
- 14) K. Shimomura, K. Nishiyama, and R. Kadono: *Phys. Rev. Lett.* **89** (2002) 255505.
- 15) E. A. Davis, S. F. J. Cox, R. L. Lichti, and C. G. Van de Walle: *Appl. Phys. Lett.* **82** (2003) 592.
- 16) K. Shimomura, R. Kadono, K. Ohishi, M. Mizuta, M. Saito, K. H. Chow, B. Hitti, and R. L. Lichti: *Phys. Rev. Lett.* **92** (2004) 135505.
- 17) S. F. J. Cox, J. S. Lord, S. P. Cottrell, J. M. Gil, H. V. Alberto, A. Keren, D. Prabhakaran, R. Scheuermann, and A. Stoykov: *J. Phys.: Condens. Matter* **18** (2006) 1061.
- 18) S. F. J. Cox, J. L. Gavartin, J. S. Lord, S. P. Cottrell, J. M. Gil, H. V. Alberto, J. P. Duarte, R. C. Vilão, N. Ayres de Campos, D. J. Keeble, E. A. Davis, M. Charlton, and D. P. van der Werf: *J. Phys.: Condens. Matter* **18** (2006) 1079.
- 19) T. U. Ito, W. Higemoto, T. D. Matsuda, A. Koda, and K. Shimomura: *Appl. Phys. Lett.* **103** (2013) 042905.
- 20) K. Shimomura and T. U. Ito: *J. Phys. Soc. Jpn.* **85** (2016) 091013.
- 21) B. R. Carroll, R. L. Lichti, P. W. Mengyan, B. B. Baker, Y. G. Celebi, P. J. C. King, K. H. Chow, and I. Yonenaga: *Appl. Phys. Lett.* **105** (2014) 122101.
- 22) X. Liu, T. S. Bjørheim, and R. Haugrud: *J. Mater. Chem. A* **5** (2017) 1050.
- 23) J. Zhang, G. Gou, and B. Pan: *J. Phys. Chem. C* **118** (2014) 17254.
- 24) T. Hanna, Y. Muraba, S. Matsuishi, N. Igawa, K. Kodama, S.-i. Shamoto, and H. Hosono: *Phys. Rev. B* **84** (2011) 024521.
- 25) Y. Kobayashi, O. J. Hernandez, T. Sakaguchi, T. Yajima, T. Roisnel, Y. Tsujimoto, M. Morita, Y. Noda, Y. Mogami, A. Kitada, M. Ohkura, S. Hosokawa, Z. Li, K. Hayashi, Y. Kusano, J. Kim, N. Tsuji, A. Fujiwara, Y. Matsushita, K. Yoshimura, K. Takegoshi, M. Inoue, M. Takano, and H. Kageyama: *Nature Mater.* **11** (2012) 507.
- 26) S. K. Estreicher: *Mater. Sci. Eng. R Rep.* **14** (1995) 319.
- 27) R. F. Kiefl, J. W. Schneider, H. Keller, W. Kündig, W. Odermatt, B. D. Patterson, K. W. Blazey, T. L. Estle, and S. L. Rudaz: *Phys. Rev. B* **32** (1985) 530(R).
- 28) J. W. Schneider, K. Chow, R. F. Kiefl, S. R. Kreitzman, A. MacFarlane, R. C. DuVarney, T. L. Estle, R. L. Lichti, and C. Schwab: *Phys. Rev. B* **47** (1993) 10193.
- 29) T. U. Ito, W. Higemoto, A. Koda, and K. Shimomura: *Appl. Phys. Lett.* **115** (2019) 192103.
- 30) K. Chow, R. Kiefl, W. MacFarlane, J. Schneider, D. Cooke, M. Leon, M. Paciotti, T. Estle, B. Hitti, R. Lichti, S. Cox, C. Schwab, E. Davis, A. Morrobel-Sosa, and L. Zavieh: *Phys. Rev. B* **51** (1995) 14762(R).
- 31) B. E. Schultz, K. H. Chow, B. Hitti, R. F. Kiefl, R. L. Lichti, and S. F. J. Cox: *Phys. Rev. Lett.* **95** (2005) 086404.
- 32) K. Momma and F. Izumi: *J. Appl. Cryst.* **44** (2011) 1272.
- 33) J. H. Brewer, S. R. Kreitzman, D. R. Noakes, E. J. Ansaldo, D. R. Harshman, and R. Keitel: *Phys. Rev. B* **33** (1986) 7813(R).
- 34) K. Nishiyama, S. Nishiyama, and W. Higemoto: *Physica B: Condens. Matter* **326** (2003) 41.
- 35) T. Lancaster, S. J. Blundell, P. J. Baker, M. L. Brooks, W. Hayes, F. L. Pratt, J. L. Manson, M. M. Conner, and J. A. Schlueter: *Phys. Rev. Lett.* **99** (2007) 267601.
- 36) R. Kadono, K. Shimomura, K. H. Satoh, S. Takeshita, A. Koda, K. Nishiyama, E. Akiba, R. M. Ayabe, M. Kuba, and C. M. Jensen: *Phys. Rev. Lett.* **100** (2008) 026401.
- 37) T. U. Ito, W. Higemoto, K. Ohishi, N. Nishida, R. H. Heffner, Y. Aoki, A. Amato, T. Onimaru, and H. S. Suzuki: *Phys. Rev. Lett.* **102** (2009) 096403.
- 38) J. Sugiyama, Y. Ikeda, T. Noritake, O. Ofer, T. Goko, M. Månsson, K. Miwa, E. J. Ansaldo, J. H. Brewer, K. H. Chow, and S.-i. Towata: *Phys. Rev. B* **81** (2010) 092103.
- 39) N. Stone: *At. Data Nucl. Data Tables* **90** (2005) 75.
- 40) S. R. Kreitzman, T. Pfiz, S. Sun-Mack, T. M. Riseman, J. H. Brewer, D. L. Williams, and T. L. Estle: *Hyperfine Interact.* **64** (1991) 561.
- 41) B. Hitti, S. R. Kreitzman, T. L. Estle, E. S. Bates, M. R. Dawdy, T. L. Head, and R. L. Lichti: *Phys. Rev. B* **59** (1999) 4918.
- 42) R. L. Lichti, S. F. J. Cox, K. H. Chow, E. A. Davis, T. L. Estle, B. Hitti, E. Mytilineou, and C. Schwab: *Phys. Rev. B* **60** (1999) 1734.
- 43) R. L. Lichti, H. N. Bani-Salameh, B. R. Carroll, K. H. Chow, B. Hitti, and S. R. Kreitzman: *Phys. Rev. B* **76** (2007) 045221.
- 44) K. H. Chow, B. Hitti, R. F. Kiefl, S. R. Dunsiger, R. L. Lichti, and T. L. Estle: *Phys. Rev. Lett.* **76** (1996) 3790.
- 45) K. H. Chow, R. F. Kiefl, J. W. Schneider, B. Hitti, T. L. Estle, R. L. Lichti, C. Schwab, R. C. DuVarney, S. R. Kreitzman, W. A. MacFarlane, and M. Senba: *Phys. Rev. B* **47** (1993) 16004(R).
- 46) K. Shimomura, P. Bakule, F. L. Pratt, K. Ohishi, K. Ishida, I. Watanabe, Y. Matsuda, K. Nishiyama, E. Torikai, and K. Nagamine: *J. Phys.: Conf. Ser.* **225** (2010) 012004.
- 47) K. Shimomura, P. Bakule, F. Pratt, K. Ishida, K. Ohishi, I. Watanabe, Y. Matsuda, K. Nagamine, E. Torikai, and K. Nishiyama: *Physics Procedia* **30** (2012) 224.
- 48) K. Yokoyama, K. Nagamine, K. Shimomura, H. W. K. Tom, R. Kawakami, P. Bakule, Y. Matsuda, K. Ishida, K. Ohishi, F. L. Pratt, I. Shiraki, and E. Torikai: *Physics Procedia* **30** (2012) 231.
- 49) B. Gu, T. Ziman, and S. Maekawa: *JPS Conf. Proc.* **2** (2014) 010301.
- 50) K. Hayashi, P. V. Sushko, Y. Hashimoto, A. L. Shluger, and H. Hosono: *Nature Commun.* **5** (2014) 3515.
- 51) J. Salasin and C. Rawn: *Crystals* **7** (2017) 143.
- 52) J. W. Akitt: *NMR and Chemistry* (Chapman & Hall, 1992) 3rd ed.
- 53) M. Hiraishi, K. M. Kojima, M. Miyazaki, I. Yamauchi, H. Okabe, A. Koda, R. Kadono, S. Matsuishi, and H. Hosono: *Phys. Rev. B* **93** (2016) 121201(R).
- 54) K. Hayashi, S. Matsuishi, T. Kamiya, M. Hirano, and H. Hosono: *Nature* **419** (2002) 462.
- 55) M. Kitano, Y. Inoue, Y. Yamazaki, F. Hayashi, S. Kanbara, S. Matsuishi, T. Yokoyama, S.-W. Kim, M. Hara, and H. Hosono: *Nature Chem.* **4** (2012) 934.
- 56) M. Kitano, S. Kanbara, Y. Inoue, N. Kuganathan, P. V. Sushko, T. Yokoyama, M. Hara, and H. Hosono: *Nature Commun.* **6** (2015) 6731.
- 57) K. Shimomura, R. Kadono, A. Koda, K. Nishiyama, W. Higemoto, and T. U. Ito: *JPS Conf. Proc.* **2** (2014) 010308.
- 58) T. U. Ito, W. Higemoto, K. Ohishi, K. Satoh, Y. Aoki, S. Toda, D. Kikuchi, H. Sato, and C. Baines: *Phys. Rev. B* **82** (2010) 014420.
- 59) J. F. Schooley, W. R. Hosler, and M. L. Cohen: *Phys. Rev. Lett.* **12** (1964) 474.
- 60) W. D. Rice, P. Ambwani, M. Bombeck, J. D. Thompson, G. Haugstad, C. Leighton, and S. A. Crooker: *Nature Mater.* **13** (2014) 481.
- 61) B. Jalan, R. Engel-Herbert, T. E. Mates, and S. Stemmer: *Appl. Phys. Lett.* **93** (2008) 052907.
- 62) R. Nakayama, M. Maesato, T. Yamamoto, H. Kageyama, T. Terashima, and H. Kitagawa: *Chem. Commun.* **54** (2018) 12439.
- 63) Z. Salman, T. Prokscha, A. Amato, E. Morenzoni, R. Scheuermann, K. Sedlak, and A. Suter: *Phys. Rev. Lett.* **113** (2014) 156801.
- 64) T. Yajima, A. Kitada, Y. Kobayashi, T. Sakaguchi, G. Bouilly, S. Kasahara, T. Terashima, M. Takano, and H. Kageyama: *J. Am. Chem. Soc.* **134** (2012) 8782.
- 65) N. Masuda, Y. Kobayashi, O. Hernandez, T. Bataille, S. Paofai, H. Suzuki, C. Ritter, N. Ichijo, Y. Noda, K. Takegoshi, C. Tassel, T. Yamamoto, and H. Kageyama: *J. Am. Chem. Soc.* **137** (2015) 15315.
- 66) Y. Tang, Y. Kobayashi, K. Shitara, A. Konishi, A. Kuwabara, T. Nakashima, C. Tassel, T. Yamamoto, and H. Kageyama: *Chem.*

- Mater. **29** (2017) 8187.
- 67) R. S. Hayano, Y. J. Uemura, J. Imazato, N. Nishida, T. Yamazaki, and R. Kubo: Phys. Rev. B **20** (1979) 850.
- 68) K. K. Baldrige and J. S. Siegel: J. Phys. Chem. A **103** (1999) 4038.
- 69) T. Tanaka, M. Abe, M. Aoki, M. Fukao, H. Inuma, Y. Ikedo, K. Ishida, T. U. Ito, M. Iwasaki, R. Kadono, O. Kamigaito, S. Kanda, D. Kawall, N. Kawamura, A. Koda, K. M. Kojima, M. K. Kubo, Y. Matsuda, T. Mibe, Y. Miyake, K. Nagamine, S. Nishimura, T. Ogitsu, R. Okubo, N. Saito, K. Sasaki, Y. Sato, S. Seo, K. Shimomura, P. Strasser, M. Sugano, K. S. Tanaka, D. Tomono, H. A. Torii, E. Torikai, A. Toyoda, K. Ueno, Y. Ueno, D. Yagi, H. Yasuda, H. Yamaguchi, A. Yamamoto, T. Yamanaka, H. Yamazaki, M. Yoshida, and T. Yoshioka: J. Phys.: Conf. Ser. **1138** (2018) 012008.